Please cite as: Franciosa P.; Serino A.; Al Botros R.; Ceglarek D.; "Closed-loop gap bridging control for remote laser welding of aluminum components based on first principle energy and mass balance"; Journal of Laser Applications 31(2):022416 - DOI: 10.2351/1.5096099, May 2019

CLOSED-LOOP GAP BRIDGING CONTROL FOR REMOTE LASER WELDING OF ALUMINIUM COMPONENTS BASED ON FIRST PRINCIPLE ENERGY AND MASS BALANCE

Pasquale Franciosa, Armando Serino, Rehab Al Botros, Darek Ceglarek

Warwick Manufacturing Group, Gibbet Hill Road, University of Warwick, Coventry CV4 7AL, UK

Abstract

Remote Laser Welding (RLW) has been successfully deployed for Steel products, particularly doors, closures and hang-on parts with overlap seam welding configurations. The growing demand for light-weight body structures has created interesting opportunities to apply RLW to fillet welding with application to Aluminium components. However, seamless migration from seam welding of Steel to fillet welding of Aluminium is limited by the following challenges: weld seam tracking capability to compensate trim edge variations; hot cracking resulting from the interaction between material chemistry and heat dissipation; form error variations leading to unwanted part-to-part gaps, which in absence of filling material must be bridged only by autogenous material.

This paper focuses on the aspect of the part-to-part gap bridging and proposes a model to select and adjust welding process parameters to control the volume of molten pool, and achieve gap bridging. The proposed model is based on the observation that gap bridging is impaired by five distinct failure modes. Each mode is modelled by first-principle energy balance criteria. Selection of welding parameters is presented by a set of *gap bridging capability* charts which helps to prevent failure modes, and select feasible weld process parameters.

Keywords: Remote Laser Welding; Aluminium Alloy; Fillet Welding; Gap Bridging; Selection of Welding Parameters.

Introduction

The introduction of ever stricter CO_2 emission targets has pushed manufactures to develop and implement effective solutions to reduce vehicle weight and optimise technical performances, such as driveability, fuel consumption and safety. OEMs have looked at different technical solutions, and among all, the adoption of multi-material body construction is considered the key enabler to have the "right material at the right place for the right performance". Aluminium alloys are certainly playing a critical role, because of their undoubtable high strength-to-density ratio, high corrosion resistance and high extrudability. Recent reports by automotive OEMs [1]–[3] show that 50 to 60% of the car body-in-white construction is currently made of Aluminium alloys. For example, Aluminium doors present significant scope for weight and cost savings. In general, an Aluminium door can be 30% lighter than an equivalent made of steel [4]. The demand of Aluminium alloys is also projected to drastically increase in the next few years due to the market push for battery electric vehicles [5]. For instance, with the increase in battery systems and their weight, extruded Aluminium frames/chassis become highly desirable as counterbalance to reduce system cost and meet vehicle performance's targets.

Laser welding technology has been proved to be a promising solution to effectively join Aluminium components. The key benefits are as follows: reduced thermal and heat affected zone, so reduced dimensional deformation and improved assembly quality; single-sided access; improved depth of fusion while reducing flange length by more than half of current standards for contact-based technology (i.e., spot welding and riveting) [6]. With conventional fixed optics (short focal length) laser welding, also called tactile laser welding, the robot needs to navigate to each seam, which penalises the overall cycle time due to non-productive robot repositions. Those reposition steps can be dramatically reduced with the introduction of remote optics (medium to long focal length) which is synchronised with the robot path [7], and able to *weld-on-the-fly*, thus minimising the overall cycle time by five times. Hence, the introduction of Remote Laser Welding (RLW) technology takes the positive features of tactile laser welding and bring additional benefits, such as increased processing speed, hence increased throughput; reduced operational cost and service, due to the reduction of auxiliary equipment such as wire feeder or shielding gas supply.

Despite all those benefits, the introduction of RLW to Aluminium components is not seamless. Key technical challenges are as follows: (1) *weld seam tracking* - in order to achieve shorter flange length to reduce body weight, it is desirable to shift from overlap seam welding to fillet welding. With tactile laser welding,

fillet welding is possible by mechanically guided probes, which track the 3D profile of the seam. However, in order to process fillet welding with RLW a fast and accurate optical detection is necessary; optical tracking is usually limited by tracking camera resolution, standing-off distance and process emissions, such as plasma plumes and spatters [8]; (2) *weld seam hot cracking* – in aluminium alloys the hot crack susceptibility depends on the content of silicon and magnesium which leads to dendrite structures due to large solidification rates [9]. Cracking occurs when the available supply of liquid metal is insufficient to fill the space between dendrites, which is opened by shrinkage strains. It has been proved [10] that the sensitivity to hot cracking can be reduced by chemically enriching the molten pool with suitable filler alloys (i.e., 5xxx series Al-Mg and/or 6xxx series Al-Si), which is the best practice today with tactile laser welding with filler wire. However, with RLW the hot cracking phenomenon cannot be controlled by acting directly on the chemistry of the molten pool because of the remote standing off distance; (3) *part-to part gap bridging* - the absence of filling material poses a key challenge to compensate manufacturing tolerances of parts being welded [11]. For example, in automotive body-in-white sheet metal assembly, form tolerances on stamped parts may raise up to ±0.5 mm. This may lead to part-to-part gaps of up to 1 mm, which, if not properly controlled, impair the integrity of the weld.

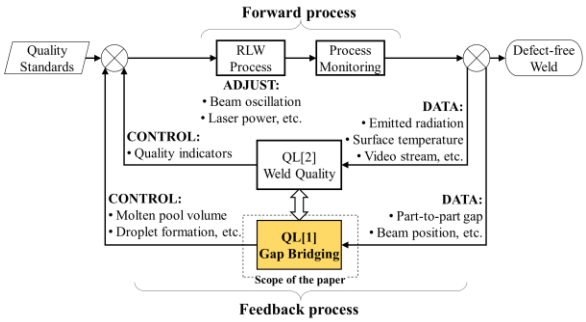

Fig. 1 Closed-Loop Quality Control system for RLW process with overlap fillet welding.

Those challenges lead to the requirement of developing a systematic *Closed-Loop In-Process* (CLIP) quality control system to achieve (near) defect-free parts. The general framework for CLIP is illustrated in Fig. 1 which hinges on two main streams: process monitoring (*forward process*), and process control and adjustment (*feedback process*) to achieve given quality requirements. Two quality loops are identified: *Gap Bridging Loop* (QL[1]); and, *Weld Quality Loop* (QL[2]), which aims at controlling the integrity of the weld quality, such as penetration, concavity/convexity, seam roughness, etc.. This paper will focus specifically on QL[1]. It is worth noting that QL[1] and QL[2] are mutually coupled – for example, weld may exhibit excessive seam roughness, even though the gap is perfectly bridged. However, this paper will decouple the two loops, and treat QL[2] as a constraint in the control architecture. Solutions to the fully-coupled problem will be explored in future works.

Part-to-part gap can be compensated for in two ways: (i) an optimised design of the clamping system; and, (ii) an adaptive gap compensation by beam oscillation and power modulation. Though the first option is the current practice today, it is prone to errors and may lead to unwanted residual stresses because of the over-constrained status of the parts. On the contrary, beam oscillation along with power modulation have been proved [12] to be an effective way for both hot cracking mitigation and part-to-part gap bridging. Beam oscillation is obtained through fast and accurate galvo scanners which are able to deflect the laser beam in fractions of seconds. Power modulation is obtained by fast modulation of the delivered laser power. Combination of beam oscillation and power modulation can be used to influence the dynamics of the molten pool, which leads to improved weldability and reduced sensitivity to surface oxide [13]. The concept of beam oscillation and power modulation has been originally introduced for electro-beam welding. Later on, it has been used for laser welding and has shown significant benefits in the stabilization of the welding process for similar but also dissimilar materials [14]. For example, Kraetzsch et al. [15] investigated the use of high frequency (>1 kHz) beam oscillation to control the degree of mixing, turbulence of molten pool, heat input and solidification rate. Both Aluminium-to-Aluminium and Aluminium-to-Copper have been studied. Sommer et al. [16] studied the use of beam oscillation for controlling penetration depth with the keyhole close to the deep-penetration threshold. Then, Langrieger et al. [17] developed a systematic hot cracking criterion based on FEM simulation of the thermo-mechanical coupling to quantify the sensitivity to hot cracking. Recently, beam oscillation and power modulation have been applied for gap bridging purposes [18], and then Muller et al. [19] reported experimental evidences. The basic idea is that as the gap size increases, more material has to be molten. Because of the missing filler wire for RLW process this material has to drop from the upper part. This is achieved by adaptively changing the beam oscillation amplitude and/or increasing the laser power. They noticed that controlling the droplet detachment is essential to create sound welds. The dynamics of the droplet in the molten pool (whose typical natural frequency of oscillation are in range of 100 to 600 Hz) is a complex process which is mostly dominated by thermal gradients - induced by conductive heat transfer

Please cite as: Franciosa P.; Serino A.; Al Botros R.; Ceglarek D.; "Closed-loop gap bridging control for remote laser welding of aluminum components based on first principle energy and mass balance"; Journal of Laser Applications 31(2):022416 - DOI: 10.2351/1.5096099, May 2019

and convective fluid flow -, liquid viscosity and surface tension and gravity load [20]. Characterisation of the droplet formation for gap bridging has been approached only via *data-driven* models. Those models use process data, gathered for example by high speed cameras, to extract correlation patterns linked to the process parameters. However, those patterns are often difficult to be fully exploited outside of the observed dataset because of changes of the physics within the molten pool. This implies that any change in welding process parameters or material properties cannot be handled by the data-driven models [21].

This paper contributes to develop a first-principle formulation of gap bridging for prompt selection and adjustment of process parameters. The paper proposes a model which aims at supporting the selection of welding process parameters in order to control the volume of the molten pool, and achieve gap bridging. The proposed model is based on the observation that gap bridging is impaired by five distinct *failure modes*. Each mode is modelled by first-principle energy balance criterion. Selection of welding parameters is presented by set of *gap bridging capability* charts which helps to avoid failure modes, and select sets of feasible process parameters. The fundamental steps to compute the gap bridging capability charts are illustrated and discussed throughout the paper.

Physical principles

Experimental configuration

A 6 kW diode laser (LDF 6000-6 LaserLine GmbH, Germany), with a beam parameter product of 6 mm·mrad was used. The laser beam was delivered through an optical fiber of 150 μm diameter and coupled with the WeldMaster Scan&Track remote welding head (YW52 Precitec GmbH, Germany), which comes with 150 mm collimating length, 300 mm focal length, and Rayleigh length of 2.76 mm. No shielding gas nor filler wire was used throughout the experiments. Samples were wiped with acetone before welding to remove surface contaminations.

Definition of process parameters

Beam oscillation is achieved by motorised mirror and collimator, integrated in standards optical components. A number of oscillation patterns are possible, such as linear, circular, single or double harmonic, etc. In order to simplify the notation, we refer only to the single harmonic pattern. Other patterns can be derived from the proposed formulation. Power modulation is obtained by analogue interface between the laser source (slave node) and the welding head (master node).

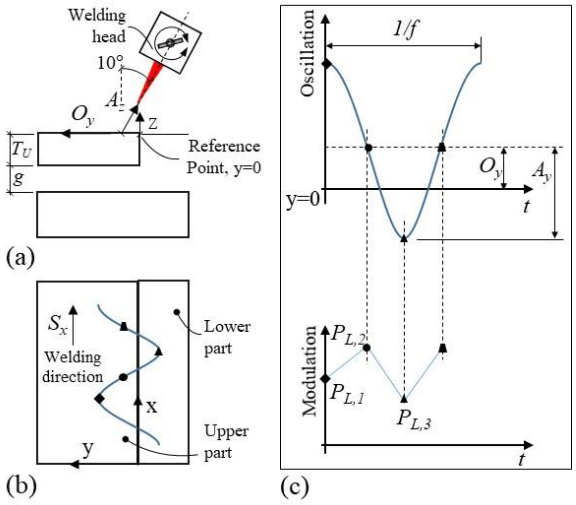

Fig. 2 Definition of KCCs. (a) cross view; (b) top view; (c) beam oscillation and power modulation.

The adopted coordinate reference system is made by (see Fig. 2): x axis refers to the welding direction; y axis is the transversal oscillation direction; z is perpendicular to both x and y; Z axis corresponds to the laser beam axis. Gap bridging is dependent upon several control parameters. Previous work [22] has shown the Key Control Characteristics (KCC) are as follows: (1) laser power, $P_{L,}$ which is modulated transversally to the welding direction; P_L is modulated on three points: $P_{L,1}$ to $P_{L,3}$, which correspond to the laser power on the upper part, reference point, and lower part, respectively; (2) oscillation amplitude, A_y, of the oscillation pattern with frequency *f*; (3) lateral offset, O_y – it is measured from the reference point, and defines the position in the y direction of the laser beam when A_y is zero; (4) focal position offset, A_z - distance along the beam axis between the focal point and the intersection of beam with the part being welded; it is zero when the focal point is on surface. Part-to-part gap, *g*, is treated as non-controllable but measurable factor. O_y, A_y and A_z are controlled through motorised optics. P_L is controlled via analogue interface.

Scope and assumptions

We assume that parts are welded in overlap fillet weld configuration, with the thinnest part always on top of the stack. Gap between parts is generated because of manufacturing tolerances of parts being welded, or because of tooling/clamping errors. Effect of inclination is neglected – parts are supposed to be always perpendicular to the gravitational load (horizontal configuration). Moreover, the incidence angle between the laser beam and the part is constant and equal to 10°; and, welding speed and oscillation frequency are set

Please cite as: Franciosa P.; Serino A.; Al Botros R.; Ceglarek D.; "Closed-loop gap bridging control for remote laser welding of aluminum components based on first principle energy and mass balance"; Journal of Laser Applications 31(2):022416 - DOI: 10.2351/1.5096099, May 2019

constant to 6 m/min, and 150 Hz, respectively. The material used in this study is SSR AA 5182 Aluminium (4.3% Mg).

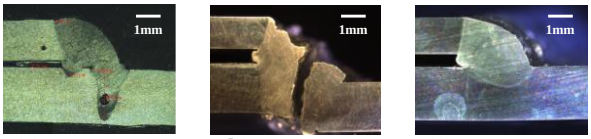

Fig. 3 Effect of power modulation. (a) constant power input; (b) excessive power at $P_{L,3}$; (c) sound weld.

In overlap fillet welding the transversal modulation of the laser power is a key parameter to control the shape of the molten pool. Because of the thickness change at the reference point (moving from upper to lower part), a constant power input leads to the so-called M-shaped weld (Fig. 3(a)), with pronounced weld root on the lower part. Excessive power input at $P_{L,3}$ generates excessive weld penetration which may turn to severe cracking (Fig. 3(b)). Therefore, the power input is decomposed into two sets as follows: $P_{L,1}$ to control the droplet formation and the volume of molten liquid on the upper part; $P_{L,2}$ and $P_{L,3}$ to control the weld root and penetration. Herein, if not otherwise stated, in order to simplify the mathematical notation, P_L is the modulated power on the upper part, $P_{L,1}$, whereas $P_{L,2}$ and $P_{L,3}$ are assumed constant to 6.0 kW and 2.5 kW, respectively. Those values have been experimentally determined to satisfy minimum 20% of weld penetration.

Experimental observations

Fig. 4(a) depicts micrograph of sound gap bridging. The smooth transition of the molten material from the upper to the lower part (Fig. 4(b)) is a symptom of sound bonding.

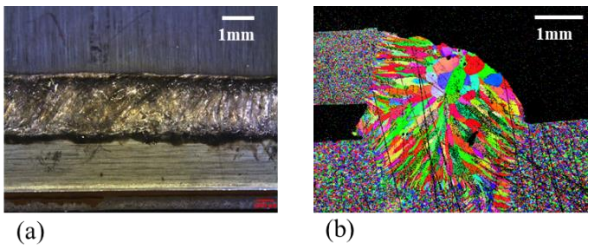

Fig. 4 Micrograph of sound gap bridging. (a) - top view; (b) - cross section (EBSD grain morphology).

The bonding mechanisms is explained by the formation and growing of the pendant droplet, as conceptually illustrated in Fig. 5. By neglecting inertia, shrinkage effects and mass flows (i.e. Marangoni effect), the formation of the droplet is driven by surface tension force and weight of the molten metal. The volume of the molten metal determines its weight, that is, gravitational load. Modulating the heat input (Fig. 5(a)) increases the amount of molten volume, which is pushed downward by its weight (formation of pendant droplet – Fig. 5(b)) until a sound bonding condition is achieved (Fig.5(c)).

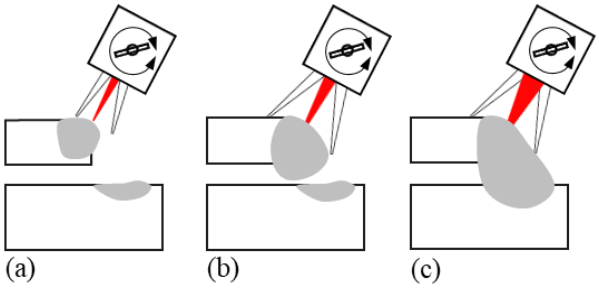

Fig. 5 Bonding mechanism. (a) - formation of the molten pool on the upper part; (b) - growing of pendant droplet; (c) - bonding between upper and lower plate.

Table 1 – Observed failure modes occurring during gap bridging.

Failure mode	Pictorial view	Experimental view
Lack of fusion **mode [1]**	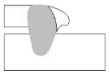	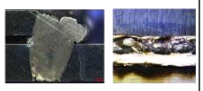
Lack of bonding (mushy regime) **mode [2]**		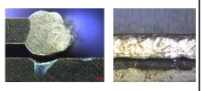
Lack of bonding (vaporisation regime) **mode [3]**	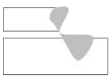	
Droplet shredding **mode [4]**	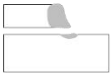	
Excessive gap **mode [5]**	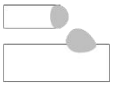	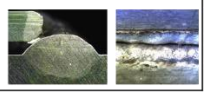

Un-controlled heat input generates faulty weld with lack of gap bridging. We have observed five distinct failure modes as shown in Table 1: mode [1] - *Lack of fusion* - the molten pool is trapped within the solid material of the upper part, and the droplet cannot be generated. Both liquid and solid metal co-exist; mode [2] - *Lack of bonding (mushy regime)* – the material is molten and the droplet is generated. However, the liquid is in the transition stage (mushy regime) just near the melting point, and the surface tension/viscosity is too high to allow successful growing of the droplet, which gets stretched only in the vertical direction; mode [3] - *Lack of bonding (vaporisation regime)* – the material is now fully molten, but has been over-heated, which leads to excessive vaporisation of the droplet; mode [4] - *Droplet shredding* - the droplet is torn down into small

Please cite as: Franciosa P.; Serino A.; Al Botros R.; Ceglarek D.; "Closed-loop gap bridging control for remote laser welding of aluminum components based on first principle energy and mass balance"; Journal of Laser Applications 31(2):022416 - DOI: 10.2351/1.5096099, May 2019

drips, which evolve primarily in the horizontal direction, transversally to the welding direction; this is explained by excessive acceleration along the y axis; mode [5] - *Excessive gap* – premature detachment of the upper droplet before bonding with the lower part; this occurs when the gravitational load overcomes surface tension force. Fig. 6 depicts the process mapping with the identified failure modes.

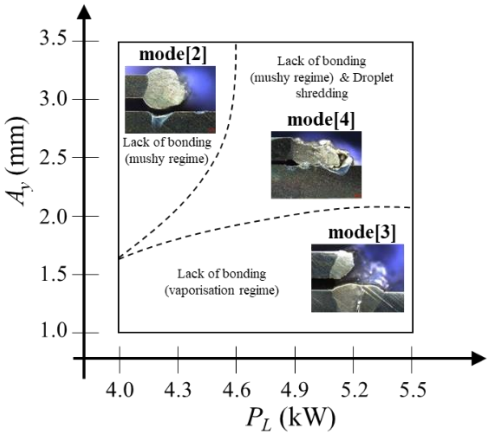

(a) O_y=0.0mm; A_z=-0.5mm; gap=0.7mm

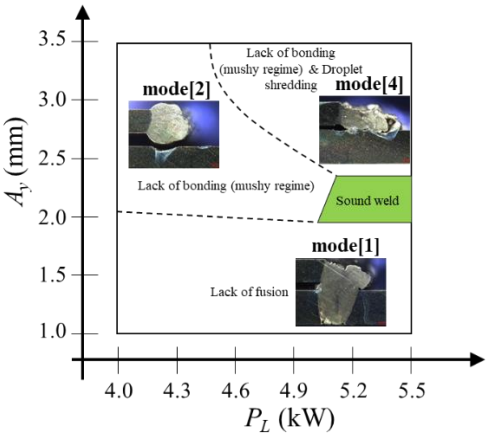

(b) O_y=0.8mm; A_z=-0.5mm; gap=0.7mm

Fig. 6 Process mapping of failure modes occurring during gap bridging. T_U=1.5 mm; T_L=2.2mm; S_x=6m/min; f=150Hz.

Model development

The key principle for selecting KCCs is that as the gap size increases, more material has to be molten from the upper part. This can be achieved by increasing A_y, and consequently laser power, P_L. However, too high A_y leads to the reduction of the interaction time, so the molten pool dynamics may drastically change and drift towards unstable and turbulent flows, as observed in mode [4]. Better control is achieved by simultaneously increasing also the lateral offset, O_y, which helps to maintain A_y to a lower value (as also observed in Fig. 6(b)). However, O_y needs to be selected in such a way the molten pool is fully developed throughout the thickness of the upper part, so to avoid mode [1]. When A_y becomes too low the welding regime turns towards the keyhole mode which tends to excessively over-heat the molten pool, as observed in mode [3]. Contrarily, if the metal is not heated up above a certain limit, it reaches only the mushy regime, as observed in mode [2], and fails to build the droplet. Based on those observations we conclude that conduction mode welding is a favourable condition to achieve a round and stable droplet on the upper part; however, this condition is not sufficient for controlling the weld penetration on the lower part. Therefore, the heat input will be modulated transversally along the y axis in order to achieve conduction regime on the upper part, and keyhole regime, if necessary, only on the lower part.

The proposed approach is developed as follows: P_L, A_y, O_y to control the gap bridging, and therefore controlling the conduction regime on the upper part; A_z to control the weld penetration, and to satisfy weld quality requirements – that is, quality loop Q[2] which is however not considered in this paper; thereby, A_z is kept constant.

Definitions

The position of the oscillating laser beam at time t is described by Equation (1), where S_x and f are the linear welding speed and the oscillation frequency, respectively.

$$\begin{cases} x = S_x t \\ y = O_y + A_y \sin(2\pi f t) \end{cases} \quad (1)$$

The derivative over time of Equation (1) gives the effective velocity components in x, V_x, and y, V_y. It could be noticed that V_y linearly increases with A_y.

$$\begin{cases} V_x = S_x \\ V_y = 2\pi f A_y \cos(2\pi f t) \end{cases}, V = \sqrt{V_x^2 + V_y^2} \quad (2)$$

The key dimensions of the molten pool are illustrated in Fig. 7. Let be y_w and y_m the width of the molten pool ($y_w = y_{w,U} + y_{w,L}$), and the instant size of the tail of the molten pool, just behind the laser spot, respectively. The shape of the instant molten pool is assumed to be symmetrical because we neglect the effect of V_x which is one order of magnitude smaller than the component in y, V_y. Furthermore, the shape of the molten pool around the turning point is wider due to energy accumulation caused by the switch of the effective velocity V_y.

Please cite as: Franciosa P.; Serino A.; Al Botros R.; Ceglarek D.; "Closed-loop gap bridging control for remote laser welding of aluminum components based on first principle energy and mass balance"; Journal of Laser Applications 31(2):022416 - DOI: 10.2351/1.5096099, May 2019

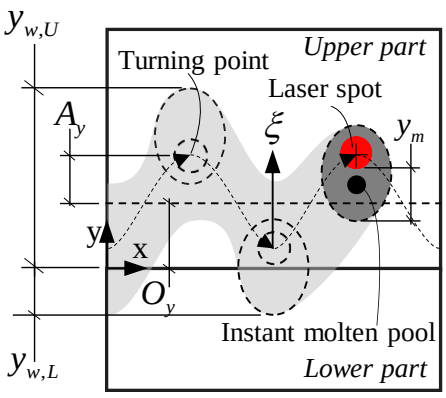

Fig. 7 Representation of molten pool along the oscillated beam path.

Assuming a Gaussian beam profile, the radius of the laser spot, R_s, is defined by the Rayleigh length, Z_R, and the radius of the spot on focus, $R_{s,f}$, as in Equation (3).

$$R_s = R_{s,f}\sqrt{1+\left(\frac{A_z}{Z_R}\right)^2} \tag{3}$$

Modelling of failure modes

Mode [1]

Mode [1] occurs when both liquid and solid co-exist nearby the edge being welded. By neglecting the edge effect on the heat dissipation (that is, the proximity of the beam to the edge may induce non-isotropic heat dissipation and non-symmetrical shapes of the molten pool), mode [1] is avoided when the position of the molten pool extends also to the bottom part. Therefore, $y_{w,L}$, which is cumulatively calculated as in Equation (4a), must be negative.

$$y_{w,L} = O_y - A_y - y_m - R_s \tag{4a}$$

Herein, if not otherwise stated, in order to maintain consistency of mathematical notation, mode avoidances are always formulated with the sign of "greater than". Mode [1] is then avoided if Equation (4b) stands.

mode[1] avoidance :

$$-\left(O_y - A_y - y_m - R_s\right) > 0 \tag{4b}$$

Mode [2] & Mode [4]

Both mode [2] and mode [4] appear because of insufficient feed of liquid to the droplet. For instance mode [2] appears when $y_{w,U}$ is below a critical limit; whereas mode [4] is the result of excessive lateral acceleration in the y direction (that is proportional to oscillation amplitude) which tends to shred the pendant droplet. Mode [2] is avoided by maintaining a conduction regime on the upper part. It has been proved that in conduction regime the width of the molten pool is approximatively double the depth [22]. Aiming to achieve full development of the molten pool throughout the thickness of the upper part, T_U, with sufficient liquid to fill the part-to-part gap, g, $y_{w,U}$ is formulated by Equation (5a).

$$y_{w,U} \geq 2\left(T_U + g\right) \tag{5a}$$

$y_{w,U}$ is cumulatively calculated as in Equation (5b),

$$y_{w,U} = O_y + A_y + y_m + R_s \tag{5b}$$

By combining Equation (5a) and (5b), mode [2] is avoided if Equation (6a) is met.

mode[2] avoidance :

$$O_y + A_y + y_m + R_s - 2\left(T_U + g\right) \geq 0 \tag{6a}$$

mode[4] avoidance :

$$2\left(T_U + g\right) - O_y - A_y - R_s > 0 \tag{6b}$$

With the increase of A_y the acceleration in y also get higher. To avoid generation of small drips in the liquid thread (that is y_m<0), and stay away from mode [4], Equation (6b) must be fulfilled. Equation (6b) is derived from Equation (6a) by forcing the condition y_m>0.

Mode [3]

Mode [3] refers to excessive over-heating of the molten pool, which tends to open the keyhole on the upper part. If the keyhole is too close to the reference corner, then the material would evaporate and reduce the feeding to the droplet. To avoid mode [3] Equation (7) stands, where y_{kh} is the width of the keyhole opening, and is computed using the formulation developed in [21].

mode[3] avoidance :

$$O_y - A_y - 0.5y_{kh} > 0 \tag{7}$$

Mode [5]

We aim to find the maximum gap which could be bridged before detachment of the droplet under the effect of gravitational force. The formation of pendant droplets is a complex mechanism which involves the equilibrium between cohesive forces (such as, surface tension, viscous forces, mass flows) and gravitational force.

Please cite as: Franciosa P.; Serino A.; Al Botros R.; Ceglarek D.; "Closed-loop gap bridging control for remote laser welding of aluminum components based on first principle energy and mass balance"; Journal of Laser Applications 31(2):022416 - DOI: 10.2351/1.5096099, May 2019

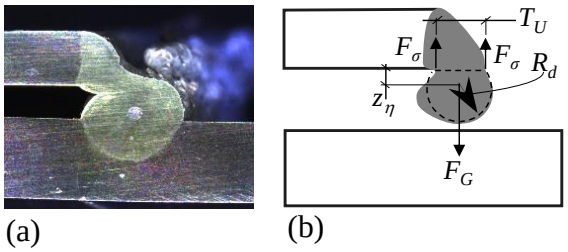

Fig. 8 Representation of droplet detachment. (a) – experimental cross section; (b) – model representation.

If we consider (see also Fig. 8) only the cohesive contribution of the surface tension, σ, (thereby, we neglect the additional elongation z_η due to the stretching and shrinkage of the droplet), the equilibrium at the static state writes as $F_G = F_\sigma$, with G the gravitational acceleration. Based on those assumption we can write that the detachment occurs when Equation (8a) is satisfied.

$$\begin{cases} F_G = mG \\ F_\sigma = 2\pi\sigma \cdot 0.5T_U \\ F_G \geq F_\sigma \end{cases} \quad (8a)$$

In Equation (8a) the neck of the droplet corresponds to T_U. This is reasonable when the molten liquid extends throughout the thickness, as imposed by the avoidance condition of mode [2]. Then, if we approximate the droplet with a spherical cap of radius R_d, the mass, m, is calculated from its density, ρ, as in Equation (8b).

$$m = \frac{4}{3}\pi R_d^3 \rho \quad (8b)$$

Combining Equation (8a) and (8b) yields to:

$$R_d \geq \sqrt[3]{\frac{3\sigma}{4G\rho}T_U} \equiv g_{\max} \quad (9)$$

which gives an estimation of the maximum bridgeable gap, g_{max}. It can be noticed that g_{max} is dependent upon material properties (surface tension and density) and the upper material thickness.

Calculation of Gap Bridging Capability

For a pre-defined maximum bridgeable gap, the *Gap Bridging Capability*, C_B, is the reassemble of those KCCs (i.e., P_L, A_y and O_y) which satisfy the necessary conditions to avoid failure mode [1] to [4] as stated in Equation (4b, 6a, 6b and 7). The methodological steps are shown in Table 2.

Table 2 – Methodological steps for calculation of gap bridging capability.

Step (1) *Define inputs*: material property; material thickness; etc.

Step (2) *Get process data*: welding speed, S_x; oscillation frequency, f; etc.

Step (3) *Compute "Gap Bridging Capability"*:
(3.1) - generate sets of *KKCs*=$\{P_L, A_y, O_y\}$
Repeat for each set of KKCs
(3.2) - compute y_m
(3.3) - check mode avoidance as per Equation (4b, 6a, 6b and 7)
(3.4) - if Equation (4b, 6a, 6b and 7) are all satisfied, then C_B=1; if not, C_B=0
Next set of KKCs

After having defined input parameters (Step (1)) and gathered process data (Step (2)), sets of KCCs are generated (Step (3.1)) within minimum and maximum limits which are dictated by manufacturing and technological requirements. For instance, A_y is limited by the stroke of the oscillating mirror; whereas P_L is capped by the installed laser power. A key role is played by y_m (Step (3.2)); it is computed using the Rosenthal equation with moving line heat source, which gives a solution to the temperature distribution, T, around the laser spot, as in Equation (10). Note is made that the approximation of line heat source is reasonable because we aim to maintain a fully developed molten pool within the upper thickness, with (near) zero thermal gradients within the thickness. In Equation (10), α is the absorption coefficient of the laser power to the material, λ is the thermal conductivity, k is the thermal diffusivity, and K_0 is the modified Bessel function of second kind and zero order [23]; and, T_a the ambient temperature. The local reference system attached to the laser spot is defined by ξ (see Fig. 7).

$$T = T_a + \frac{\alpha P_L}{2\pi\lambda}\exp\left(-\frac{V}{2k}\xi\right)K_0\left(\frac{V}{2k}|\xi|\right) \quad (10)$$

Equation (10) can be rearranged to calculate y_m which is reached when T equates the melting temperature, T_m.

$$y_m \equiv |\bar{\xi}| : \begin{cases} T_m - T_a - \dots \\ \dots - \frac{\alpha P_L}{2\pi\lambda}\exp\left(-\frac{V_{\max}}{2k}\bar{\xi}\right)K_0\left(\frac{V_{\max}}{2k}|\bar{\xi}|\right) = 0 \\ \bar{\xi} \leq 0 \end{cases} \quad (11)$$

V_{max} is the maximal effective velocity which, as per Equation (2), is reached when t=0. Equation (11) is non-linear and a solution can be obtained, for example,

Please cite as: Franciosa P.; Serino A.; Al Botros R.; Ceglarek D.; "Closed-loop gap bridging control for remote laser welding of aluminum components based on first principle energy and mass balance"; Journal of Laser Applications 31(2):022416 - DOI: 10.2351/1.5096099, May 2019

using the Newton-Raphson technique. In Step (3.3) violations of Equation (4b, 6a, 6b and 7) are evaluated. The calculation is made possible by the value of y_m obtained in Step (3.2) and the pre-defined maximum bridgeable gap, g_{max}, which substitutes g in Equation 6a and 6b. Then, in Step (3.4) C_B is updated, accordingly. For instance, C_B=0 implies that the gap bridging cannot be achieved; that is, violation of Equation (4b, 6a, 6b and 7), leading to an infeasible solution. On the other hand, C_B=1 corresponds to sound bridging condition; that is, Equation (4b, 6a, 6b and 7) are all met simultaneously.

Results and discussion

The proposed model has been validated through experimental trials. Model parameters used for the study are listed in Table 3. Density and surface tension have been assumed dependent upon temperature [24].

Table 3 – Model properties

Parameter	Value	Unit
Density, ρ	$2600-0.285T$	Kg/m^3
Surface tension, σ	$781-0.155(T-T_m)$	mN/m
Thermal conductivity, λ	150	W/(K·m)
Thermal diffusivity, k	63.82	mm^2/s
Melting temperature, T_m	923	K
Ambient temperature, T_a	293	K
Absorption coefficient, α	0.1	--

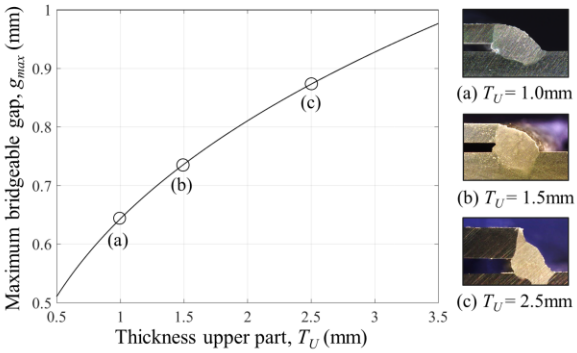

Fig. 9 Thickness vs. maximum bridgeable gap.

Fig. 9 shows the relationship between thickness of the upper part and maximum bridgeable gap, as expressed by Equation (9). For T_U=1.5 mm, the maximum gap is about 0.72mm, which corresponds to ~50% of T_U.

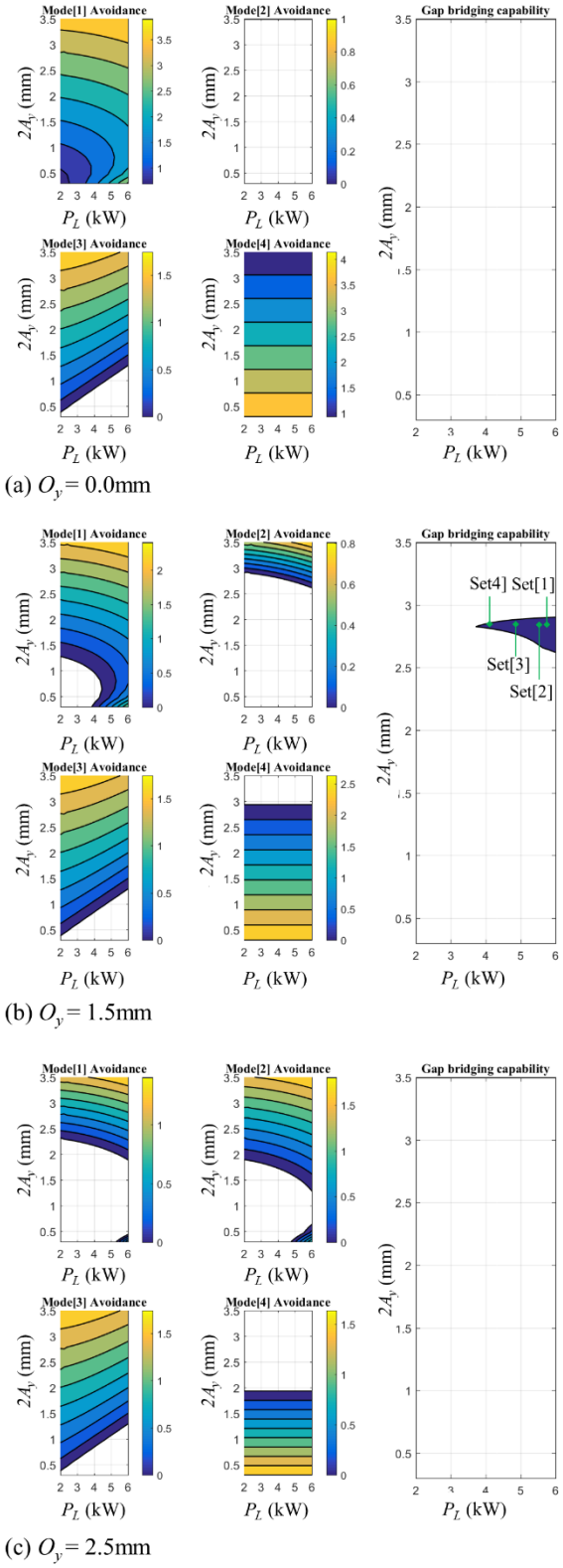

Fig. 10 Gap bridging capability for T_U=1.5mm; A_z=2.0mm; g_{max}=0.72mm; S_x=6m/min; f=150Hz.

This result is also confirmed by [8]. An interesting note is that with the increasing of thickness, g_{max} tends to reach a plateau. This indicates that bridging part-to-part gaps is more challenging for thicker materials, because, in order for the droplet to be fully established within the upper material, the weight induced by increased molten volume tends to rapidly overcome the cohesive surface tension, thus leading to a stretched droplet. For example, though a sound gap bridging is achieved for T_U=2.5 mm, the weld exhibits a pronounced reduced leg length which, among all, impairs the strength.

Fig. 10 illustrates the gap bridging capability chart and the related conditions for fault mode avoidance, according to Equation (4b, 6a, 6b and 7). The empty/blank areas for the mode avoidance chart and gap bridging capability chart correspond to a violation of Equation (4b, 6a, 6b and 7) and C_B=0, respectively. Higher values in the mode avoidance chart correspond to safer welding parameters, which are desirable to avoid gap bridging failures. It could be noticed that the feasible region is very narrow and strongly dependent upon the lateral offset O_y. For O_y=0.0 mm (Fig. 10(a)), mode [2] is predominant; whereas for O_y=2.5 mm (Fig. 8(c)) every mode exhibits infeasible solutions. Only for O_y=1.5 mm (Fig. 10(b)) a narrow feasible region is observed in the gap bridging capability chart. In principle the feasible region is a reassemble of infinite weld configurations. The selection of a specific configuration may be driven not only by gap bridging but also by weld quality requirements. This is a positive aspect that provides flexibility when coupling the gap bridging loop, QL[1], to the weld quality loop, QL[2].

Table 4 - Validation trials for for T_U=1.5mm; A_y=2.7mm; O_y=1.5mm; A_z=2.0mm; g_{max}=0.72mm; S_x=6m/min; f=150Hz.

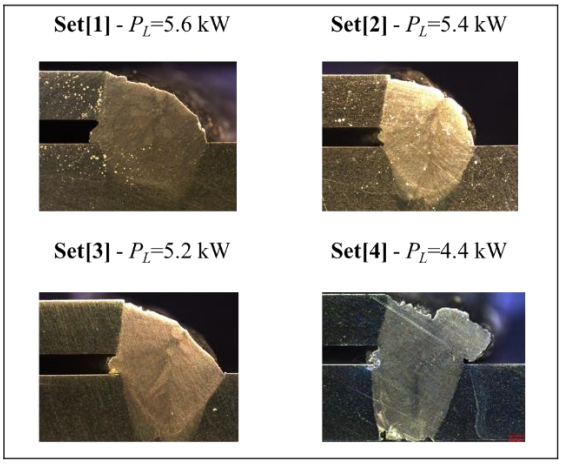

As example, Table 4 reports few micrographs generated from within the feasible region as in Fig. 10(b). Set[1] to 3 show a sound bridging condition. However, Set[4] falls to mode [1] failure, which the model is unable to predict. This is imputed to the fast solidification rates within the molten pool and transient-state, which the model does not consider at the moment.

Conclusions and next steps

A first principle model has been developed for selecting welding process parameters to control the volume of molten pool, and achieve gap bridging with application of remote laser welding with Aluminium parts.

The key principle for gap bridging is the formation of a pendant droplet which is fed by the molten liquid on the upper part. When the droplet comes in touch to the bottom part a sound bridging is achieved. Thus, controlling the volume of the molten liquid is the key to control the gap bridging. Experimental observations have suggested that the favourable condition for gap bridging is the conduction regime. Therefore, process parameters have been decoupled in two sets: in-plane control of heat input to control molten pool on the upper part; out-of-plane control to achieve desired weld penetration. This paper has focused on the first aspect.

The model is based on the observation that the gap bridging fails under five distinct modes. Each mode is modelled with mass and energy balance criteria, in steady-state condition. Those modes are condensed into a single index, named *gap bridging capability*, which helps to avoid failure modes, and select sets of feasible weld process parameters.

Results have shown that the model gives reasonable approximation of the welding modes and enables the selection of feasible welding parameters. The benefits of the model are as follows: (1) to speed-up the selection of process parameters, which in today best practice takes up to few months of experimentation. The model may help to reduce the number of physical experiments; (2) capability for automatic process adjustment by linking failure modes to welding parameters; (3) real-time closed-loop gap bridging control with automatic selection of feasible process parameters.

Further improvements are necessary to capture the transient-state which involves viscosity forces and solidification rates with phase change. Also, effect of part inclination and welding speed, and integration with quality loop will be investigated in future research.

Acknowledgements

This study was supported by the WMG Centre High Value Manufacturing Catapult (HVMC), Advanced Propulsion Centre (APC) UK and the EPSRC UK

project EP/K019368/1: Self-Resilient Reconfigurable Assembly Systems with In-process Quality Improvement.

References

[1] E. Schubert, M. Klassen, I. Zerner, C. Walz, and G. Sepold, "Light-weight structures produced by laser beam joining for future applications in automobile and aerospace industry," *J. Mater. Process. Technol.*, vol. 115, no. 1, pp. 2–8, 2001.

[2] M. Schmidt, P. Lindahl, and O. Andersson, "Joining of the XC60 Car Body," in *Automotive Circle - Joining in Car Body Engineering*, 2018.

[3] D. Husmann, "Innovations in Joining: the Body in White Structure of the new AUDI A8," in *Automotive Circle - Joining in Car Body Engineering*, 2018.

[4] P. Franciosa, S. Chatterjee, and D. Ceglarek, "Closed-Loop Quality Control System for Remote Laser Welding of Aluminium BIW Components: Current Development and Future Strategy," in *Automotive Circle - Joining in Car Body Engineering*, 2018.

[5] McKinsey&Company, "Lighweight, High Impact," *2012*.

[6] D. Ceglarek *et al.*, "Rapid Deployment of Remote Laser Welding Processes in Automotive Assembly Systems," *CIRP Ann. - Manuf. Technol.*, vol. 64, pp. 389–394, 2015.

[7] W. Vogl and F. Oefele, "Remote Welding of Fillet Seams: Coaxial seam tracking enables new approach for remote laser welding," *Laser Tech. J.*, vol. 5, pp. 39–41, 2014.

[8] P. Fixemer, F. Albert, P. Sievi, and T. Graham, "Seam Guided Laser Remote Welding with Automated Gap Bridging: Increased Process Windows by Online Recognition of Gap Situation," *Laser Tech. J.*, pp. 38–41, 2015.

[9] H. Langrieger, F. Krafft, M. Mensinger, and F. Oefele, "Fundamental analysis of hot cracks in remote laser welded aluminium fillet welds," in *Lasers in Manufacturing Conference 2015*, 2015.

[10] P. Kah, E. Hiltunen, and J. Martikainen, "Investigation of Hot Cracking in the Welding of Aluminium Alloys (6005 & 6082)," in *63rd Annual Assembly & International Conference of International Institute of Welding*, 2010.

[11] V. Schultz, T. Seefeld, and F. Vollertsen, "Gap bridging Ability in Laser Beam Welding of Thin Aluminum Sheets," *Phys. Procedia*, vol. 56, pp. 545–553, 2014.

[12] C. Thiel, A. Hess, R. Weber, and T. Graf, "Stabilization of Laser Welding Procesees by means of Beam Oscillation," in *Proceedings of SPIE*, 2012, no. May 2012.

[13] F. Albert, P. Marben, and T. Graham, "Remote Laser Welding of Steel and Aluminum Alloys: Influence of Process Parameters on Gap Bridging and Seam Roughness," *Laser Tech. J.*, pp. 32–35, 2017.

[14] H. Kotadia, P. Franciosa, and D. Ceglarek, "Challenges and Opportunities in Remote Laser Welding of Steel to Aluminium," in *The Proceedings of the 71st International Institute of Welding (IIW) Annual Assembly and International Conference*, 2018.

[15] M. Kraetzsch, J. Standfuss, A. Klotzbach, J. Kaspar, and B. Brenner, "Laser Beam Welding with High-Frequency Beam Oscillation: Welding of Dissimilar Materials with Brilliant Fiber Lasers," *Phyisics Procedia*, vol. 12, pp. 142–149, 2011.

[16] M. Sommer, J.P. Weberpals, S. Muller, and T. Graf, "Advantages of Laser Beam Oscillation for Remote Welding of Aluminum Closely above the Deep-Penetration Welding Threshold," *J. Laser Appl.*, vol. 29, 2017.

[17] H. Langrieger, F. Krafft, M. Mensinger, and F. Oefele, "Thermomechanical Analysis of the Formation of Hot Cracks in Remote Laser Welded Aluminium Fillet Welds," *J. Laser Appl.*, vol. 28, no. 2, 2016.

[18] B. Johan, A. B. Pathiraj, and R. G. K. M. Aarts, "Seam Gap Bridging of Laser ased Processes for the Welding of Aluminium Sheets for Industrial Applications," *Int J Adv Manuf Technol.*, pp. 143–154, 2010.

[19] A. Müller, S. Goecke, P. Sievi, F. Albert, and M. Rethmeier, "Laser Beam Oscillation Strategies for Fillet Welds in Lap Joints," *Phys. Procedia*, vol. 56, pp. 458–466, 2014.

[20] V. V Semak *et al.*, "Melt Pool Dynamics during Laser Welding," *J. Phys. Dyn.*, vol. 28, 1995.

[21] E. C. Ozkat, P. Franciosa, and D. Ceglarek, "Development of Decoupled Multi-physics Simulation for Laser Lap Welding Considering Part-to-Part Gap," *J. Laser Appl.*, vol. 29, no. 2, 2017.

[22] A. Serino, "Development of Closed-Loop Gap Bridging Architecture for Remote Laser Welding of 5xxx Series Aluminium Alloy," 2018.

[23] A. Kaplan, "A model of deep penetration laser

welding based on calculation of the keyhole profile," *J. Appt. Phys*, vol. 27, no. 27, pp. 1805–1814, 1994.

[24] M. Leitner, T. Leitner, A. Schmon, K. Aziz, and G. Pottlacher, "Thermophysical Properties of Liquid Aluminum," *Metall. Mater. Trans. A*, vol. 48, no. 6, pp. 3036–3045, 2017.

Meet the Authors

Dr Pasquale Franciosa is Senior Researcher at University of Warwick and CIRP research associate. His focus is process monitoring, closed loop control, machine learning, multi-disciplinary optimization, with specific attention for automotive assembly systems and laser joining technology. He has published over 70 papers and received several best paper awards. He has been coordinating and managing the technical development of several academic and industrial-driven projects. Currently, he is responsible for the development and application of remote laser welding solutions to similar and dissimilar materials. He serves on the editorial board of the ASTM SSME journal, and committees of several international conferences.

Mr Armando Serino is Project Engineer at Warwick Manufacturing Group (WMG), University of Warwick, UK. He earned his Master and Bachelor degrees in Aerospace Engineering from the University of Naples Federico II, Italy. In 2017 he received his training in the areas of optics system and process monitoring of laser welding; and, high-power diode laser system. Currently, his research area is focused on remote laser welding process and in-process quality improvement.

Dr Rehab Al Botros is a Research Fellow at Warwick Manufacturing Group, University of Warwick. She obtained her PhD from the University of Warwick, 2015. Her background is in surface characterisation, imaging techniques and finite element method modelling. Her research focuses on manufacturing process monitoring and control, and characterisation of laser welding joints for quality improvement. She is author and co-author of several papers, published in international peer-reviewed journals.

Professor Darek Ceglarek is EPSRC Star Research Chair at University of Warwick and CIRP Fellow. Previously, he was Professor in Industrial and Systems Engineering at University of Wisconsin. His research focuses on digital manufacturing, in-process quality control and root cause analysis. He has published over 150 papers and received several Best Paper Awards. He served as Chair of the Quality, Statistics and Reliability Section of INFORMS; Program Chair for the ASME Design-for-Manufacturing Life Cycle Conferences, Associate Editor of the IEEE Trans. on Automation Science and Engineering, ASME Trans, Journal of Manufacturing Science & Engineering, ASTM Smart and Sustainable Manufacturing Systems.